Detection of mitotic neuroblasts provides additional evidence of steady state neurogenesis in the adult enteric nervous system

Anastazja M. Gorecki[1, 2*], Jared Slosberg[3*], Su Min Hong[4], Blake Migden[4], Anton Gulko[5], Alpana Singh[6], Chengxiu Zhang[6], Rohin Gurumurthy[6], Subhash Kulkarni[4, 7#]

[1]Perron Institute for Neurological and Translational Science, Nedlands, Australia.

[2]School of Biological Sciences, University of Western Australia, Crawley, Australia.

[3]Department of Genetic Medicine, Johns Hopkins University – School of Medicine, Baltimore, MD, USA

[4]Division of Gastroenterology, Dept of Medicine, Beth Israel Deaconess Medical Center, Boston, MA 02115

[5]Division of Endocrinology, Dept of Medicine, Beth Israel Deaconess Medical Center, Boston, MA 02115

[6]Center for Neurogastroenterology, Department of Medicine, Johns Hopkins University – School of Medicine, Baltimore, MD USA

[7]Division of Medical Sciences, Harvard Medical School, Boston, MA 02115

*Co-first authors

[#]Address all correspondence to:

Subhash Kulkarni, Ph.D.

skulkar1@bidmc.harvard.edu

Abstract:

Maintenance of normal structure of the enteric nervous system (ENS), which regulates key gastrointestinal functions, requires robust homeostatic mechanisms, since by virtue of its location within the gut wall, the ENS is subject to constant mechanical, chemical, and biological stressors. Using transgenic and thymidine analogue-based experiments, we previously discovered that neuronal turnover – where continual neurogenesis offsets ongoing neuronal loss at steady state – represents one such mechanism. Although other studies confirmed that neuronal death continues into adulthood in the enteric nervous system (ENS), the complicated nature of thymidine analogue presents challenges in substantiating the occurrence of adult neurogenesis. Therefore, it's vital to employ alternative, well-recognized techniques to substantiate the existence of adult enteric neurogenesis in the healthy gut. Here, by using established methods of assessing nuclear DNA content and detecting known mitotic marker phosphor-histone H3 (pH3) in Hu^+ adult ENS cells, we show that ~10% of adult myenteric Hu^+ cells show evidence of mitosis and hence are cycling neuroblasts. We also show that proportions of Hu^+ cycling neuroblasts in the adult ENS neither vary with ganglia size, nor do they differ significantly between two intestinal regions – duodenum and ileum, or between sexes. The presence of a significant population of cycling neuroblasts in adult ENS provide further evidence of steady state neurogenesis in the adult ENS.

Introduction:

The cells of the enteric nervous system (ENS) are located entirely within the gut wall and are routinely exposed to significant and continual mechanical, chemical, and biological insults (1-3). Despite these ongoing and significant stressors, the question of how the adult ENS maintains itself has not been adequately addressed, especially given prior reports that a significant proportion of enteric neurons undergo apoptosis at steady state (4-6).

In a previous study, we reported the presence of a neurogenic mechanism, which gives rise to a significant number of new neurons at steady state in the adult gut (7). Using thymidine analogue studies and multiple lines of evidence to test for neuronal apoptosis, we had demonstrated the existence of an adult enteric neurogenic program that generates new neurons to replace dying apoptotic neurons, which account for ~10% of all myenteric neurons at any given time, thus maintaining the structural and functional integrity of the adult ENS. While other studies provide independent validation of the high rate of neuronal apoptosis in the adult ENS (6, 8-11), the complicated nature of thymidine-analogue based assays and their susceptibility to variations in tissue handling and fixation has made it difficult for investigators to consistently detect neurogenesis (12). Thus, there is a need to use alternate methods that can aid in the detection of adult neurogenesis and provide further evidence of a high rate of neurogenesis that counteracts the equally high rate of neuronal apoptosis.

In addition, we and others also recently showed the presence of significant heterogeneity in myenteric ganglia (13, 14). Myenteric ganglia exist in various sizes, as defined by their neuronal numbers, and in the small intestine can contain from 3 to 150 neurons (13). The relative distribution of ganglia size in the intestine was skewed significantly towards smaller ganglia (i.e. containing fewer neurons) (13). Similarly, proportions of various neuronal subpopulations contained within these ganglia show significant differences across regions of the intestine (14). This heterogeneity begs the question of whether the rates of neurogenesis and neuronal loss are

equally represented in the diverse ganglia of myenteric plexus in differing locations in the small intestine, and across the two sexes. Since thymidine analogue-based assays, which detect the presence of these chemicals dosed to animals over several days, do not permit the study of ongoing neurogenesis at a defined snapshot of time, these assays are unsuitable for providing a real time assessment of putative differences in neurogenic niches across ganglia and locations. Further, since thymidine analogues cannot be administered to human beings, these assays cannot be translated to human tissues. Thus, there is a need to simplify the protocols to facilitate better assessment of neurogenesis both in mice and in human specimens.

To address these issues, in this report, first by using a flow cytometry-based DNA content analyses and second by using an established mitotic marker phosphor-histone H3 (pH3), we identified the presence of mitotic Hu-immunolabeled cells in the adult ENS. By performing a flow cytometry-based estimation of DNA content in myenteric Hu-immunolabeled nuclei, we observe DNA content suggestive of S-phase and G2/M phase in significant proportions of Hu-immunolabeled nuclei – thus indicating active DNA synthesis and mitosis in a population of adult murine myenteric neurons. By enumerating the proportions of pH3-immunoreactive mitotic neurons, we found that the prevalence of mitotic neurons in healthy tissue matches the rate of neurogenesis previously established using thymidine analogues. Additionally, separate experiments identify subsets of human adult enteric neurons that demonstrate immunoreactivity to pH3 or to the apoptosis marker Cleaved Caspase 3 (CC3), providing evidence that these processes occur in the adult human gut. Finally, the proportions of pH3-immunoreactive neurons were found to be conserved between myenteric ganglia regardless of their size, location in the small intestine, and the sex of the animals.

Methods:

Animals: Experimental protocols were approved by The Johns Hopkins University's Animal Care and Use Committee and the Animal Care and Use Committee at Beth Israel Deaconess Medical

Center, in accordance with the guidelines provided by the National Institutes of Health. Age matched 2 – 3-month-old adult wildtype C57BL/6 mice were used.

Isolation and immunolabeling of neuronal nuclei from adult longitudinal muscle – myenteric plexus (LM-MP) tissue: Mice were anesthetized with isoflurane and sacrificed by cervical dislocation. For small intestinal tissue isolation, a laparotomy was performed, and the entire small intestine was removed and lavaged with PBS containing penicillin-streptomycin (Pen-Strep; Invitrogen). The small intestine was then cut into 1-cm-long segments. Next, tissues were placed over a sterile plastic rod and a superficial longitudinal incision was made along the serosal surface and the LM-MP was peeled off from the underlying tissue using a wet sterile cotton swab(7) and directly frozen in liquid nitrogen and stored at -80°C for further processing. Two different protocols were used hence-forth, which are detailed as follows.

BIDMC protocol: Frozen tissue was next transferred to a gentleMACs C-Tube (Miltenyi Inc.) containing with 2 ml of TST buffer (containing 60 μl of 5M NaCl, 42 μl of 1M $MgCl_2$, 20 μl of 1M Tris HCl pH 7.5, 2 μl of 1M $CaCl_2$, 10 μl 2% Bovine Serum Albumin (BSA), 6 μl 10% Tween-20, in 1860 μl ultrapure water) and allowed to thaw for 2 minutes. Thawed tissues were chopped using dissecting scissors for 45 seconds, and then added to the C-tube, which is installed on the gentleMACs dissociator (Miltenyi Inc.). The tissue was processed through two rounds of 268 rotations, for a total of 72 seconds dissociation time after which the tube was placed and incubated on ice for 10 min. Next, using a wide-bore, low retention 1000 μl pipette tip, the suspension was transferred to a 40 μm pre-wet cell sieve that was set on top of a 50 ml falcon tube and filtered through. The C-tube was washed with 1 ml of 1X ST buffer (TST buffer minus BSA and Tween-20), and the buffer was next transferred to the cell sieve. The cell sieve was then washed with 2 ml of 1X ST buffer and then discarded. Using again the wide-bore low retention 1000 μl pipette tip, the filtered nuclei suspension was transferred to a pre-wet 40 μm cell sieve that is set on top

of a 5 ml FACS tube. The suspension was spun down in a swing bucket centrifuge at 500g for 5 minutes and at 4°C. Centrifuge brake was set at half to ensure that the pellet is not disturbed. The top ~4.9 ml of the supernatant was removed, and the pellet was washed with 5 ml PBS solution containing 0.02% BSA, which was added to the tube gently and the tube was again spun at 500g for 5 minutes and at 4°C. The supernatant was removed, and the nuclear pellet was resuspended in 500 μl of PBS containing 0.02% BSA. The suspension was then split equally into two tubes. The directly conjugated antibody Anti-Hu 488 (1:750, Abcam# ab237234) was added to the first tube, while the second tube served as the control. A drop of NucBlue (Thermofisher) was added to both the tubes. Both the tubes were incubated on ice for 45 minutes, after which the nuclear suspensions were spun down at 500g for 5 minutes and at 4°C, with the centrifuge brakes again set to half. 450 μl of supernatant from each tube was removed and the nuclear pellet was resuspended in 450 μl of PBS solution containing 0.02% BSA. The suspensions were then analyzed for NucBlue fluorescence intensity (as a marker for DNA content) in Hu-immunofluorescent nuclei using the CytoFLEX flow cytometer.

JHU protocol: Frozen and chopped tissue was placed into an ice-cold gentleMACS C-tube with 3 ml of TST buffer. Tissue was dissociated on a gentleMACS Octo Dissociator using the *4C_nuclei_01* protocol with pre-chilled OctoCooler. Disrupted cell suspension was subsequently incubated on ice for 5 min before being filtered through a 40 μm pre-wet (with 1X ST buffer) cell sieve that is set on top of a 50 ml falcon tube. The C-tube was rinsed with 1 ml ST buffer and an additional 2 ml of 1X ST buffer was used to rinse the filter. The nuclei suspension was centrifuged in a swing bucket centrifuge at 500g for 5 minutes and at 4°C with the centrifuge brakes set to half. The pellet was resuspended in 5 ml PBS containing 1% BSA, centrifuged and pelleted again, and finally resuspended in PBS containing 1% BSA and 5% normal goat serum (NGS). This suspension was incubated on ice for 5 minutes after which the suspension is divided equally into two tubes. Anti-Hu 647 directly conjugated antibody (Abcam, ab237235) was added at a

concentration of 1:250 to the first but not the second tube and both the tubes are incubated on ice for 45 minutes. Excess antibody was removed by washing the suspension twice (again with centrifugation at 500g for 5 minutes and at 4°C with the centrifuge brakes set to half) and the nuclei suspensions were finally suspended in 1 ml sterile PBS in a 15 ml conical tube. Next, a fixative was freshly prepared by adding 50 μl of 50 mg/ml dithiobis(succinimidyl propionate) (DSP) in dimethyl sulfoxide (DMSO) solution to 4 ml of ice-cold methanol, dropwise while vortexing at moderate speed. The nuclei suspensions were fixed by adding the freshly prepared fixative dropwise to the nuclei, while swirling the suspension to reduce clumping. The fixed nuclei were next incubated at 4°C for 10 minutes on an end-over-end rotor (speed of 15 rpm). Fixed nuclei were rehydrated by adding 2 volumes of PBS containing 0.1% Triton-X, and then washed twice with PBS containing 1% BSA. DAPI was added to both tubes at a concentration of 1 μg/ml, and samples were filtered through a 40 μm before analyses on a flow analyzer (BD FACSAria III).

Flow data was analyzed on Flowjo 10.

Tissue preparation: Mice were anesthetized with isoflurane and sacrificed by cervical dislocation. For small intestinal tissue isolation, a laparotomy was performed, and the entire small intestine was removed and lavaged with PBS containing penicillin-streptomycin (Pen-Strep; Invitrogen), then cut into 2-cm-long segments, such that segments from duodenum, jejunum, and ileum were separated. Next, tissues were placed over a sterile plastic rod and a superficial longitudinal incision was made along the serosal surface and the longitudinal muscle containing myenteric plexus (LM-MP) was peeled off from the underlying tissue using a wet sterile cotton swab (7) and placed in Opti-MEM medium (Invitrogen) containing Pen-Strep. The tissue was then laid flat and fixed with freshly prepared ice cold 4% paraformaldehyde (PFA) solution for 4-5 minutes in the dark. All LM-MP tissues were fixed within 30 minutes of sacrifice. After the fixation, the tissue was stored in ice cold sterile PBS with Pen-Strep for immunofluorescence staining and subsequent microscopy.

Immunochemistry: For murine tissue: The fixed LM-MP tissue was washed twice in ice-cold PBS in the dark at 16°C. The tissue was incubated in blocking-permeabilizing buffer (BPB; 5% normal goat serum with 0.3% Triton-X) for 1 hour, followed by incubation with either the combination of anti-pH3 antibody (Unconjugated antibody EMD Milipore # 06-570, 1:500; Conjugated antibody, Cell Signaling #CST3458S; 1:250) and ANNA-1 (1:1000; patient antisera against the neuronal Hu antigens), or of anti-Cleaved Caspase 3 (#Asp175, Cell Signaling, 1:250) and ANNA-1(1:1000) for 48 h at 16°C in the dark with shaking at 55 rpm. The tissues were then washed three times (15-min wash each) in PBS at room temperature in the dark and incubated in the appropriate secondary antibody (Anti-human 488 and Anti-rabbit 647, Invitrogen, both at 1:500) at room temperature for 1 hour while on a rotary shaker (65 rpm). The tissues were again washed three times in PBS at room temperature, counterstained with DAPI to stain the nuclei, overlaid with Prolong Antifade Gold mounting medium, cover-slipped, and imaged.

For formalin fixed paraffin embedded (FFPE) human tissue: Use of commercially procured human tissue was approved by the Institutional Review Board of the Beth Israel Deaconess Medical Center. FFPE tissue sections of human small intestinal tissue were procured through a commercial vendor (Precision for Medicine). To process them, slides were first baked at 55°C for 15 minutes, after which, they were deparaffinized and rehydrated by immersion through the following solutions: 1) Two washes (5 minutes each) with Xylene; 2) two washes with 100% ethanol (5 minutes each); 3) two washes with 95% ethanol (5 minutes each); 4) two washes with 70% ethanol (5 minutes each); and finally 6) two washes with deionized water (5 minutes each). Next, using Sodium Citrate buffer (pH 6.0), 40-minute antigen retrieval was performed in a pressure cooker. The slides were then cooled in ice-cold 1X PBS. Slides were marked with a hydrophobic pen around the sections, and then blocked and permeabilized in BPB for 1 hour. Buffer was washed off with 1X PBS and sections were incubated with either the combination of directly conjugated anti-pH3 antibody (EMD Milipore, 1:250) and directly conjugated anti-Hu

antibody (1:300), or the combination of anti-Cleaved Caspase 3 (CC3; 1:250) and ANNA-1 (1:500) for 24 h at 16°C in the dark. For tissue sections treated with anti-CC3 and anti-ANNA1 antibodies, following incubation with primary antibody, the sections were washed three times for 15-minutes each in PBS at room temperature in the dark, then incubated with the appropriate secondary antibodies (Invitrogen Anti-human 488 and Anti-rabbit 647; both at 1:500) at room temperature for 1 hour. Next, the sections were again washed three times in PBS at room temperature, counterstained with DAPI to stain the nuclei, overlaid with Prolong Antifade Gold mounting medium, cover-slipped, and imaged.

Microscopy: Microscopy was performed using the oil immersion 40X objective on the Olympus Fluoview 3000rs confocal microscope with galvano and resonance scanning mode, and with 20X magnification of the EVOS M7000 microscope. Control tissues that were immunostained with secondary antibodies only were used to set the threshold laser intensities. In mice, all ANNA-1/Hu-immunostained neurons were included in the analysis.

Results:

Adult murine small intestinal myenteric neurons show evidence of mitosis.

First, we used flow cytometry-based estimation of DNA content in Hu-immunolabeled nuclei to test whether a significant proportion of myenteric Hu^+ nuclei show presence of higher than the expected 2N DNA content, which would suggest the presence of cells in S-phase (DNA replication) and in G2/M phase (mitosis) of the cell cycle. On performing this assay on >10,000 unfixed Hu-immunolabeled nuclei derived from LM-MP tissues from adult healthy mice that were housed in the barrier facility at BIDMC, we observed that >10% of these Hu^+ nuclei show evidence of higher-than-expected DNA content, which indicates that these cells undergo DNA replication and mitosis (Fig 1a, b, c). Based on DNA content, 2.68% of all Hu^+ nuclei were found to be in S-phase and 10.7% were found to be in G2/M phase of the cell cycle. We next tested whether the

observation of >2N DNA content in myenteric Hu^+ nuclei was dependent on fixation or housing conditions. For this, Hu-immunolabeled fixed nuclei that were derived from small intestinal LM-MP tissue of adult healthy mice housed in a non-barrier facility at Johns Hopkins University were analyzed and were again found to have 3.16% of all Hu^+ nuclei were found to be in S-phase and 9.47% were found to be in G2/M phase of the cell cycle (Fig 1d). Thus, we establish a high degree of concordance in the proportions of Hu^+ cells in S and G2/M phase of cell cycle in adult mice, irrespective of their housing conditions and colony location, as well as whether the nuclei were stained with or without fixation.

Next, we further tested the presence of mitosis in adult enteric Hu^+ cells by microscopic detection of an established mitotic marker phosphor-histone H3 in the neurons of the myenteric plexus (15-19). By using antibodies against the protein phosphor-Histone H3 (pH3; phosphorylated at residue Ser10, which occurs at the initiation of the G2 phase and continues into metaphase), we observed that the adult healthy small intestinal LM-MP tissue derived from mice housed in the Johns Hopkins University mouse colony contains diverse cell populations of pH3-immunostained cells that are present both within and outside of the myenteric ganglia (Fig 2a, b). Importantly, using the unconjugated pH3 antibody and the anti-Hu ANNA-1 antisera, we observe that the pH3-positive, intra-ganglionic cell population comprises of Hu-immunostained cells (Fig 2a, b), as well as other unlabeled cells that we assume to be populations of proliferating enteric glial cells (20) and enteric neuronal precursor cells, that we have previously shown to express Nestin and Ki-67 (7). Using conjugated pH3 and Hu antibodies, we tested whether adult myenteric ganglia in mice housed in the barrier facility at BIDMC also similarly contained pH3-immunoreactive Hu^+ cells (Fig 2c). Similar to our earlier observations (7), Cleaved Caspase 3 (CC3) immunoreactivity, which indicates apoptotic cells, was found restricted to a subset of myenteric Hu^+ cells (Fig 2d).

Human small intestinal myenteric ganglia show evidence of neuronal turnover. We next tested whether the adult human small intestinal myenteric plexus tissue also shows evidence of

significant cell proliferation through the presence of pH3-immunoreactive Hu^+ cells. In immunolabeled FFPE tissue sections, by using directly conjugated antibody against pH3, we found that many cells in the longitudinal muscle layer of human gut wall also showed immunoreactivity against the mitosis marker pH3 (Fig 3a). By co-immunostaining these FFPE tissue sections with directly conjugated antibodies against pH3 and Hu, we found that many pH3 immunoreactive cells were found in the myenteric ganglia, some of which were also immmunolabeled by antibodies against Hu (Fig 3b), providing evidence that our observations of pH3 and Hu co-immunoreactivity in adult murine small intestinal myenteric cells also extend to adult human small intestinal myenteric cells. Immunostaining FFPE tissues with unconjugated pH3 antibody and anti-Hu ANNA-1 antisera also identified a subset of pH3+ Hu^+ myenteric cells (Fig 3c). Similarly, we also found that the apoptotic marker Cleaved Caspase 3 was detected in a subset of human small intestinal myenteric neurons (Fig 3d), while the negative control for CC3 immunoreactivity (performed without primary antibody) showed no background signal (Fig 3e).

Significant proportions of adult small intestinal myenteric Hu^+ cells are mitotic. Since co-immunolabeling with antibodies against pH3 and pan-neuronal marker Hu (Fig 2) provides evidence of mitosis in adult small intestinal myenteric Hu^+ cells, we next quantified the proportions of pH3-immunoreactive mitotic small intestinal myenteric Hu^+ cells at steady state in adult mice. By confocal microscopy, we observed 2577 Hu-immunolabeled Hu^+ cells from the small intestines of 6 adult healthy male and female mice (n = 3 of either sex), which included myenteric plexus tissue from both duodenum and ileum. We found that 8.54% ± 1.09 (mean ± SEM) of all Hu-immunolabeled cells also showed co-immunolabeling with anti-pH3 antibodies (Fig 4a,b).

Next, we analyzed whether pH3 immunoreactivity in Hu^+ cells from the ileum or duodenal myenteric ganglia showed any sex bias. In the duodenal myenteric ganglia, we counted 670 Hu^+ cells in tissues from female mice and 601 Hu^+ cells in the tissues from male mice (n = 3 of either sex), and found no significant difference between the percentage of pH3-immunoreactive Hu^+

cells between the two sexes (mean ± SEM pH3$^+$ neurons: female mice = 11.63 ± 2.00; male mice = 6.26 ± 0.75; p = 0.17, Unpaired t-test with Welch's correction, Fig 4a). In the ileal myenteric ganglia, we counted 667 Hu$^+$ cells in the tissues from female mice and 639 Hu$^+$ cells in the tissues from male mice (n = 3 of either sex), and found no significant difference between the percentage of pH3-immunoreactive Hu$^+$ cells between the two sexes (mean ± SEM pH3$^+$ neurons: female mice = 9.93 ± 0.92; male mice = 6.82 ± 0.34; p = 0.06, Unpaired t-test with Welch's correction, Fig 4b). Finally, we compared pH3 immunoreactivity in populations of Hu$^+$ cells between ileum vs the duodenal tissue across the two sexes and found no significant difference (Duodenal tissue: Hu$^+$ cells counted = 1271, mean ± SEM pH3$^+$ Hu$^+$ cells: 8.64 ± 1.52; Ileal tissue: Hu$^+$ cells counted = 1306, mean ± SEM pH3$^+$ Hu$^+$ cells: 8.38 ± 0.82; p = 0.88, Unpaired t-test with Welch's correction, Fig 4c).

We have previously shown that there is significant heterogeneity in ganglia size, demonstrated by small intestinal myenteric ganglia containing as few as 3 neurons or over 100 neurons(13). Here, we tested whether proportion of mitotic Hu$^+$ cells correlate with ganglia size in the adult healthy small intestinal myenteric plexus. By analyzing the proportions of pH3-immunoreactive Hu$^+$ cells in 147 ganglia of various sizes (3 – 56 neurons per ganglia) from duodenum and ileum from 6 mice together, we found an absence of any significant correlation between percent Hu$^+$ cells immunoreactive for pH3 in myenteric ganglia and the numbers of Hu$^+$ cells within ganglia (ganglia size) (D'Agonistino and Pearson test for normality showed non-normal distribution, non-parametric Spearman correlation test: r = -0.05625 p = 0.5; Fig 4d).

We next tested whether there was any correlation between ganglia size and the proportions of CC3-immunoreactive apoptotic Hu$^+$ cells in the adult healthy murine small intestinal myenteric plexus. We quantified the percent of CC3-immunoreactive Hu$^+$ cells from 83 myenteric ganglia from 3 mice, where the myenteric ganglia size ranged from 3 – 58 neurons. We found that the proportion of CC3$^+$ Hu$^+$ cells in small intestinal myenteric ganglia increased significantly with

ganglia size (D'Agonistino and Pearson test for normality showed non-normal distribution, non-parametric Spearman correlation test: $r = 0.4181$ $p < 0.0001$; Fig 4e).

Discussion:

Using established flow cytometry and immunolabeling based assays (15-19, 21-23), our report provides evidence that a significant proportion of Hu^+ ganglionic cells in the small intestinal myenteric plexus tissue from adult mice undergo mitosis. Neurogenesis from precursor cells requires DNA replication and mitosis, and the detection of mitosis and apoptosis in Hu-immunolabeled cells in healthy small intestinal myenteric plexus tissue shows that there is ongoing genesis of new neurons in this organ, which offsets the continual loss of neurons to apoptosis. Our prior study, which used thymidine analogue-based assays to demonstrate that almost 90% of adult small intestinal neurons were generated during a 2-week period, had suggested that ~10% of neurons are generated (and hence are newborn) on any given day (7). Here, our DNA content-based flow cytometry analysis shows that ~10% of Hu-immunolabeled myenteric nuclei showed evidence of DNA content associated with G2/M (or mitotic) phase of the cell cycle, which is in line with our microscopy-based data that again demonstrate ~10% of Hu-immunolabeled cells within myenteric ganglia express the mitotic marker phosphor-histone H3 (pH3). Thus our observation of ongoing mitosis in Hu-immunolabeled cells using these two different methods closely matches the rate of neurogenesis we had previously deduced using detection of thymidine analogues (7). In addition, the presence of pH3 can be readily detected in Hu-immunolabeled ganglionic cells in the adult human gut – further suggesting that a similar neurogenic process is also present in the adult human gut. We again confirm that a subpopulation of adult murine small intestinal myenteric neurons showed detectable presence of the apoptotic marker Cleaved Caspase 3 (CC3) (7).

Evidence of DNA replication (S-phase) and mitosis (G2/M phase) in Hu-immunolabeled cells suggests that in addition to being a marker for mature functional neurons, Hu is also expressed

by cycling neuroblasts or transit amplifying cells that are committed to a neuronal fate. Thus, rather than suggesting that adult enteric neurons are mitotic in nature, we infer that Hu immunoreactivity is not restricted to mature neurons. This argument is supported by prior studies that have shown that Hu is expressed in neuronally committed cycling progenitors or neuroblasts as well as in immature neurons (24, 25). The presence of a significant population of cycling Hu^+ neuroblasts in the adult myenteric plexus provides evidence of a robust steady state neurogenic process in the adult gut.

The thymidine analogue-based assay we had previously deployed to observe adult enteric neurogenesis requires complicated methods (12). In addition, by virtue of being based on the uptake, incorporation, and accumulation of these chemicals over time into newly synthesized nucleic acids, this assay can neither sensitively measure the ongoing rate of DNA synthesis and cell proliferation at any given point of time, nor can it be used to assess rate of neurogenesis in humans. By using the flow analyses and microscopy-based methods, we provide a simple established assay to robustly measure the proportions of cycling neuroblasts in tissue to infer the rate of neurogenesis at health, in disease, or in response to interventions in the adult human and murine gut.

In light of our recent study that provides evidence that the post-natal ENS consists of neurons derived from two developmental lineages (26), observations reported here suggest a new model for adult enteric neurogenesis (Fig 5). In this model, since ~90% of adult enteric neurons were found to be newborn over a 2-week period (7), we propose that populations of both neural crest-derived enteric neurons (NENs) and the mesoderm-derived enteric neurons (MENs) undergo steady state neurogenesis in adults. This suggests that there are two separate lineage-associated populations of enteric neuronal precursor cells in the adult ENS – one for NENs (that co-express Nestin and p75NTR), and another for MENs, whose exact molecular identity currently remains unknown (26). While NEN and MEN precursors generate distinct populations of neuroblasts (26-

28), whether Nestin expression is restricted only to neuroblasts of the NEN lineage is currently unknown. The model proposes that neuroblasts from both lineages expand and continually generate Hu^+ mature neurons to maintain the myenteric neuronal numbers. Our model postulates that the rate of neurogenesis matches the rate of neuronal loss in both lineages in the adult healthy gut and further research is needed to study whether the rate of neuronal turnover is different between the lineages in the healthy and diseased gut.

The immunohistochemical analyses of mitotic neuroblasts and apoptotic neurons in the murine small intestinal myenteric plexus also allowed us to test whether neurogenesis and neuronal loss - the two processes driving neuronal turnover - occur equally in all myenteric ganglia across two different small intestinal regions and between the two sexes. Taking the proportions of mitotic neuroblasts to mature neurons as a measure of the neurogenic activity for each ganglion, we provide evidence that neurogenic activity does not significantly differ between differently sized ganglia, between two different intestinal regions, or between sexes. However, while the rate of neurogenesis does not change across ganglia, we observe that larger ganglia (i.e. with greater number of neurons) have a higher percentage of neurons undergoing apoptosis. If neurogenesis occurs at a uniform rate across all ganglia, then the observation that apoptosis occurs more frequently in larger ganglia implies that there may be a regulatory process that discourages the preservation or further enlargement of these larger ganglia. This is reflected in our prior findings that showed that smaller ganglia are much more frequent than larger ganglia in the adult small intestinal myenteric plexus tissue (13). This suggests that the balance between the genesis and death of neurons within ganglia is crucial for regulating the ganglia size. Furthermore, it would indicate that any disruptions to this balance, whether through increased neurogenesis or elevated neuronal death, could alter the normal proportions of smaller and larger ganglia, potentially leading to disorders in intestinal movement. While whether such a ganglia size-associated skew in genesis and loss of neurons extends to human tissue is still unknown, a recent study by

Boschetti et al. (29) shows that patients with dysmotility have significantly reduced neuronal numbers in myenteric ganglia (or that the presence of larger ganglia in their ENS is greatly reduced). These are similar to the observations made by Bernardini et al. (30) who showed that myenteric ganglia of patients with ulcerative colitis had significantly fewer numbers of neurons, when compared to healthy controls. These observations suggest that ganglionic rate of neurogenesis and of neuronal loss may change in disease to alter the ENS structure. While our study did not aim to provide a quantitative measure of neurogenesis and neuronal loss in the adult human gut, we show that mitotic pH3-immunolabeled neuroblasts and apoptotic CC3-immunolabeled neurons exist in the adult human gut. These findings, together with those of Chandrasekharan et al. (9) and of Kozlowska et al. (4, 5), who showed the presence of a significant proportion of apoptotic myenteric neurons in the adult human gut, provide evidence that a cellular program of neuronal turnover also occurs in human gut. Further studies are needed to establish the rate of neuronal turnover in the adult human ENS and interrogate whether alteration in this rate is associated with alterations in ENS structure and disease.

Our study is robust as it establishes concordance of our observations based on two different experiments - the DNA content-based flow analyses experiments, and the pH3-based immunohistochemical experiments, which were performed on adult mice from two different institutions. Thus, this study further confirms the presence of the homeostatic mechanism of steady state neuronal turnover in the adult ENS.

Acknowledgements: SK was supported by an R01 grant from the National Institute of Aging (R01AG66768) and a pilot award from the Diacomp foundation. AG was supported by a Fulbright Future Scholarship, funded by The Kinghorn Foundation. J.S. was funded through the Maryland Genetics, Epidemiology, and Medicine training program sponsored by the Burroughs Welcome Fund.

Figure Legends

Figure 1: Evidence of S and G2/M phases of cell cycle in a population of Hu-immunolabeled cells from the small intestinal myenteric plexus tissue of adult healthy mice. Flow analyses of nuclei isolated from the Longitudinal muscle and myenteric plexus tissue (LM-MP) from adult healthy mice housed in a barrier facility at BIDMC, when immunolabeled with directly conjugated anti-Hu 488 antibody and co-stained with a DNA-binding dye NucBlue, show that (a) significant proportion of events present with detectable NucBlue-labeling and hence are annotated as nuclei. This population of isolated nuclei contains (b) >10K nuclei with detectable immunolabeling with the anti-Hu antibody and is hence annotated as Hu^+ nuclei. (c) Using fluorescence intensity of DNA dye NucBlue as a marker for DNA content, analyses of DNA content within the Hu-immunolabeled nuclei reveals that while 74.2% of nuclei have DNA content (2N) expected in the G1 phase cells, 2.68% of Hu^+ nuclei contain DNA content that corresponds to cells in S-phase (DNA replication phase); and 10.7% of Hu^+ nuclei contain DNA content that corresponds to cells in G2/M phase (Mitotic phase). The enumeration of nuclei does not include those that show less than 2N DNA content, which we assume reflects apoptotic neurons. (d) Flow analysis of nuclei isolated from LM-MP of similarly aged mice housed in at Johns Hopkins University, which were immunolabeled with anti-Hu 647 antibody post-fixation and were stained with the DNA dye DAPI show the presence of 86.3% of nuclei have DNA content (2N) expected in the G1 phase cells, 3.16% of Hu^+ nuclei contain DNA content that corresponds to cells in S-phase (DNA replication phase); and 9.47% of Hu^+ nuclei contain DNA content that corresponds to cells in G2/M phase (Mitotic phase).

Figure 2: Cell proliferation marker phospho-histone H3 (pH3) is detected in neurons and other cells of the adult healthy myenteric plexus tissue. Confocal microscopy shows that the (a) Longitudinal muscle and myenteric plexus tissue (LM-MP) from an adult healthy mouse that was housed at Johns Hopkins University, when stained with unconjugated antibodies against phospho-Histone H3 (pH3, red) and the pan-neuronal marker Hu (green) shows the presence of pH3 immunoreactivity in ganglionic cells that do express Hu (yellow arrow) and those that don't express Hu (cyan arrow). pH3 immunoreactivity is also detected in extra-ganglionic cells in this tissue (white arrow) that are presumed to be longitudinal muscle cells. (b) Magnified image of a myenteric ganglia labeled with antibodies against pH3 (red) and Hu (green) again show the presence of pH3-immunoreactive Hu-immunolabeled new-born neurons (yellow arrow), along with neurons that are not immunoreactive against pH3 (white arrow) and pH3-immunoreactive extra-ganglionic cells (cyan arrow). (c) *Left:* Representative image of LM-MP tissue from an adult mouse housed in the barrier facility at BIDMC when stained with directly conjugated antibody against pH3 (red) shows the presence of significant pH3-immunoreactivity in the tissue. The tissue was also co-immunostained with directly conjugated anti-Hu antibody and the region of interest (white box) when magnified shows (*Right*) the presence of Hu-immunolabeled (green) neurons that co-label for pH3. Nuclei are stained with DAPI (blue). (d) Representative image of the adult murine small intestinal LM-MP tissue, when stained with antibodies against Cleaved Caspase 3 (CC3, red) and the pan-neuronal marker Hu (green), shows the presence of CC3 immunoreactivity in a subset of Hu-immunoreactive neurons (yellow arrows), while other neurons in the same and other ganglia do not immunolabel for CC3 (green arrow). Nuclei are labeled with DAPI (blue). Scale bar indicates 10 μm.

Figure 3: New-born and apoptotic neurons exist in human small intestinal myenteric ganglia. (a) Cells of the longitudinal muscle layer of the human gut wall in formalin fixed paraffin embedded (FFPE) tissue sections from adult human small intestine with immunolabelling of mitotic marker pH3 (red) and co-staining with DAPI (blue) show detectable pH3 immunoreactivity in many cells of this tissue. Image created by stitching contiguous 40X images of the section which was imaged with the EVOS M7000 microscope. (b) Co-immunolabeling adjacent sections of this tissue with directly conjugated antibodies against mitotic marker pH3 (red) and pan-neuronal marker Hu (green) and by imaging them with the M7000 microscope, we observe the presence of pH3-immunoreactive cells that also immunolabel with antibodies against Hu (yellow arrows). (c) Confocal microscopy of FFPE human tissues that were immunolabeled with anti-Hu ANNA-1 antisera and anti-pH3 antibody and then suitably co-stained with secondary antibodies again show the presence of pH3 and Hu co-labeled cells within the myenteric ganglia (yellow arrow). (d) Orthogonal views generated from confocal microscopy of a myenteric ganglia immunostained with antibodies against CC3 (red) and anti-Hu ANNA-1 (green) show the presence of CC3-immunolabeled neurons. (e) Representative image of a myenteric ganglia immunostained with antibodies against Hu (green) but no primary antibodies for the red channel shows a lack of non-specific staining with the secondary antibodies. Photomicrographs in panels (c – e) were generated by confocal microscopy. Nuclei are labeled with DAPI (blue) and scale bar in (c – e) indicates 10 μm.

Figure 4: Quantifications of pH3-immunoreactive and CC3-immunoreactive Hu^+ cells in the adult murine gut. (a) Quantification of pH3-immunoreactive Hu^+ cells in the duodenal tissue of age-matched male and female mice show no significant sex-bias in their proportions ($p > 0.05$, Students' t-test). (b) Quantification of pH3-immunoreactive Hu^+ cells in the ileal tissue of age-matched male and female mice show no significant sex-bias in their proportions ($p > 0.05$, Students' t-test). (c) Quantification of pH3-immunoreactive Hu^+ cells in the duodenal and ileal tissue of age-matched mice show no significant differences in their proportions between the two tissue regions ($p > 0.05$, Students' t-test). (d) Distribution of percent pH3-immunoreactive Hu^+ cells in small intestinal ganglia containing various numbers of Hu^+ cells. (e) Cubic curve fit (black line) for the distribution of CC3-immunoreactive Hu^+ cells in small intestinal ganglia containing various numbers of Hu^+ cells.

Figure 5: New model of neuronal turnover in the adult gut. The data presented in this manuscript, when viewed in perspective of our earlier data on adult steady state neurogenesis (7) and the presence of two neuronal lineages in the adult gut (26) helps us build a new model for neuronal turnover in the adult gut. In this model, the adult ENS contains two different enteric neural precursor cell (ENPC) populations – one for NEN lineage, which expresses markers Nestin and p75NTR, and another for MEN lineage (whose exact molecular signature is currently unknown). The ENPCs, which do not express the marker Hu, give rise to the population of Hu-expressing neuroblasts that also express the mitotic marker pH3. Together these comprise ~10% of all Hu-immunolabeled cells in the LM-MP layer. How do the neuroblasts of the two neuronal lineages differ in terms of their molecular signature is currently unclear. These neuroblasts further differentiate to generate mature NENs and MENs that also express Hu, and which in time are fated for programmed cell death through the apoptotic pathway, at which time they express the apoptotic marker Cleaved Caspase 3 (CC3).

References

1. **Gregersen H, and Kassab G**. Biomechanics of the gastrointestinal tract. *Neurogastroenterol Motil* 8: 277-297, 1996.
2. **Sherman MP, Zaghouani H, and Niklas V**. Gut microbiota, the immune system, and diet influence the neonatal gut-brain axis. *Pediatr Res* 77: 127-135, 2015.
3. **Hyland NP, and Cryan JF**. Microbe-host interactions: Influence of the gut microbiota on the enteric nervous system. *Dev Biol* 417: 182-187, 2016.
4. **Kozlowska A, Kozera P, Majewski M, and Godlewski J**. Co-expression of caspase-3 or caspase-8 with galanin in the human stomach section affected by carcinoma. *Apoptosis* 23: 484-491, 2018.
5. **Kozlowska A, Kwiatkowski P, Oponowicz A, Majewski M, Kmiec Z, and Godlewski J**. Myenteric plexuses atrophy in the vicinity of colorectal cancer tissue is not caused by apoptosis or necrosis. *Folia Histochem Cytobiol* 54: 99-107, 2016.
6. **Nezami BG, Mwangi SM, Lee JE, Jeppsson S, Anitha M, Yarandi SS, Farris AB, 3rd, and Srinivasan S**. MicroRNA 375 mediates palmitate-induced enteric neuronal damage and high-fat diet-induced delayed intestinal transit in mice. *Gastroenterology* 146: 473-483 e473, 2014.
7. **Kulkarni S, Micci M-A, Leser J, Shin C, Tang S-C, Fu Y-Y, Liu L, Li Q, Saha M, and Li C**. Adult enteric nervous system in health is maintained by a dynamic balance between neuronal apoptosis and neurogenesis. *Proceedings of the National Academy of Sciences* 201619406, 2017.
8. **De Schepper S, Verheijden S, Aguilera-Lizarraga J, Viola MF, Boesmans W, Stakenborg N, Voytyuk I, Schmidt I, Boeckx B, Dierckx de Casterle I, Baekelandt V, Gonzalez Dominguez E, Mack M, Depoortere I, De Strooper B, Sprangers B, Himmelreich U, Soenen S, Guilliams M, Vanden Berghe P, Jones E, Lambrechts D, and Boeckxstaens G**. Self-Maintaining Gut Macrophages Are Essential for Intestinal Homeostasis. *Cell* 175: 400-415 e413, 2018.
9. **Chandrasekharan B, Anitha M, Blatt R, Shahnavaz N, Kooby D, Staley C, Mwangi S, Jones DP, Sitaraman SV, and Srinivasan S**. Colonic motor dysfunction in human diabetes is associated with enteric neuronal loss and increased oxidative stress. *Neurogastroenterology & Motility* 23: 131-e126, 2011.
10. **Becker L, Nguyen L, Gill J, Kulkarni S, Pasricha PJ, and Habtezion A**. Age-dependent shift in macrophage polarisation causes inflammation-mediated degeneration of enteric nervous system. *Gut* 67: 827-836, 2018.
11. **Ye L, Li G, Goebel A, Raju AV, Kong F, Lv Y, Li K, Zhu Y, Raja S, He P, Li F, Mwangi SM, Hu W, and Srinivasan S**. Caspase-11-mediated enteric neuronal pyroptosis underlies Western diet-induced colonic dysmotility. *J Clin Invest* 130: 3621-3636, 2020.
12. **Kulkarni S, and Pasricha PJ**. Detecting Adult Enteric Neurogenesis in the Context of Adult ENS Homeostasis. *Cell Mol Gastroenterol Hepatol* 14: 967, 2022.
13. **Kobayashi Y, Bukowski A, Das S, Espenel C, Gomez-Frittelli J, Wagle N, Bakshi S, Saha M, Kaltschmidt JA, Venkataraman A, and Kulkarni S**. COUNTEN, an AI-Driven Tool for Rapid and Objective Structural Analyses of the Enteric Nervous System. *eneuro* 8: ENEURO.0092-0021.2021, 2021.

14. **Hamnett R, Dershowitz LB, Sampathkumar V, Wang Z, Gomez-Frittelli J, De Andrade V, Kasthuri N, Druckmann S, and Kaltschmidt JA**. Regional cytoarchitecture of the adult and developing mouse enteric nervous system. *Current Biology*.
15. **Kim Y-J, Ketter R, Steudel W-I, and Feiden W**. Prognostic Significance of the Mitotic Index Using the Mitosis Marker Anti–Phosphohistone H3 in Meningiomas. *American Journal of Clinical Pathology* 128: 118-125, 2007.
16. **Rotelli MD, Policastro RA, Bolling AM, Killion AW, Weinberg AJ, Dixon MJ, Zentner GE, Walczak CE, Lilly MA, and Calvi BR**. A Cyclin A-Myb-MuvB-Aurora B network regulates the choice between mitotic cycles and polyploid endoreplication cycles. *PLoS Genet* 15: e1008253, 2019.
17. **Tiede S, Meyer-Schaller N, Kalathur RKR, Ivanek R, Fagiani E, Schmassmann P, Stillhard P, Hafliger S, Kraut N, Schweifer N, Waizenegger IC, Bill R, and Christofori G**. The FAK inhibitor BI 853520 exerts anti-tumor effects in breast cancer. *Oncogenesis* 7: 73, 2018.
18. **Uguen A, Conq G, Doucet L, Talagas M, Costa S, De Braekeleer M, and Marcorelles P**. Immunostaining of phospho-histone H3 and Ki-67 improves reproducibility of recurrence risk assessment of gastrointestinal stromal tumors. *Virchows Archiv* 467: 47-54, 2015.
19. **Jiang YH, Zhu Y, Chen S, Wang HL, Zhou Y, Tang FQ, Jian Z, and Xiao YB**. Re-enforcing hypoxia-induced polyploid cardiomyocytes enter cytokinesis through activation of beta-catenin. *Sci Rep* 9: 17865, 2019.
20. **Zeisel A, Hochgerner H, Lonnerberg P, Johnsson A, Memic F, van der Zwan J, Haring M, Braun E, Borm LE, La Manno G, Codeluppi S, Furlan A, Lee K, Skene N, Harris KD, Hjerling-Leffler J, Arenas E, Ernfors P, Marklund U, and Linnarsson S**. Molecular Architecture of the Mouse Nervous System. *Cell* 174: 999-1014 e1022, 2018.
21. **Kim KH, and Sederstrom JM**. Assaying Cell Cycle Status Using Flow Cytometry. *Current Protocols in Molecular Biology* 111: 28.26.21-28.26.11, 2015.
22. **An Z, Sabalic M, Bloomquist RF, Fowler TE, Streelman T, and Sharpe PT**. A quiescent cell population replenishes mesenchymal stem cells to drive accelerated growth in mouse incisors. *Nat Commun* 9: 378, 2018.
23. **Alonso-Martin S, Aurade F, Mademtzoglou D, Rochat A, Zammit PS, and Relaix F**. SOXF factors regulate murine satellite cell self-renewal and function through inhibition of beta-catenin activity. *Elife* 7: 2018.
24. **Seki T, Hori T, Miyata H, Maehara M, and Namba T**. Analysis of proliferating neuronal progenitors and immature neurons in the human hippocampus surgically removed from control and epileptic patients. *Scientific Reports* 9: 18194, 2019.
25. **Ekonomou A, Savva GM, Brayne C, Forster G, Francis PT, Johnson M, Perry EK, Attems J, Somani A, Minger SL, Ballard CG, Medical Research Council Cognitive F, and Ageing Neuropathology S**. Stage-specific changes in neurogenic and glial markers in Alzheimer's disease. *Biol Psychiatry* 77: 711-719, 2015.
26. **Kulkarni S, Saha M, Slosberg J, Singh A, Nagaraj S, Becker L, Zhang C, Bukowski A, Wang Z, Liu G, Leser J, Kumar M, Bakhshi S, Anderson M, Lewandoski M, Vincent E, Goff LA, and Pasricha PJ**. Age-associated changes in lineage composition of the enteric nervous system regulate gut health and disease. eLife Sciences Publications, Ltd, 2023.

27. **Bott CJ, Johnson CG, Yap CC, Dwyer ND, Litwa KA, and Winckler B**. Nestin in immature embryonic neurons affects axon growth cone morphology and Semaphorin3a sensitivity. *Mol Biol Cell* 30: 1214-1229, 2019.
28. **De Vadder F, Grasset E, Manneras Holm L, Karsenty G, Macpherson AJ, Olofsson LE, and Backhed F**. Gut microbiota regulates maturation of the adult enteric nervous system via enteric serotonin networks. *Proc Natl Acad Sci U S A* 115: 6458-6463, 2018.
29. **Boschetti E, Malagelada C, Accarino A, Malagelada JR, Cogliandro RF, Gori A, Bonora E, Giancola F, Bianco F, Tugnoli V, Clavenzani P, Azpiroz F, Stanghellini V, Sternini C, and De Giorgio R**. Enteric neuron density correlates with clinical features of severe gut dysmotility. *Am J Physiol Gastrointest Liver Physiol* 317: G793-G801, 2019.
30. **Bernardini N, Segnani C, Ippolito C, De Giorgio R, Colucci R, Faussone-Pellegrini MS, Chiarugi M, Campani D, Castagna M, Mattii L, Blandizzi C, and Dolfi A**. Immunohistochemical analysis of myenteric ganglia and interstitial cells of Cajal in ulcerative colitis. *J Cell Mol Med* 16: 318-327, 2012.

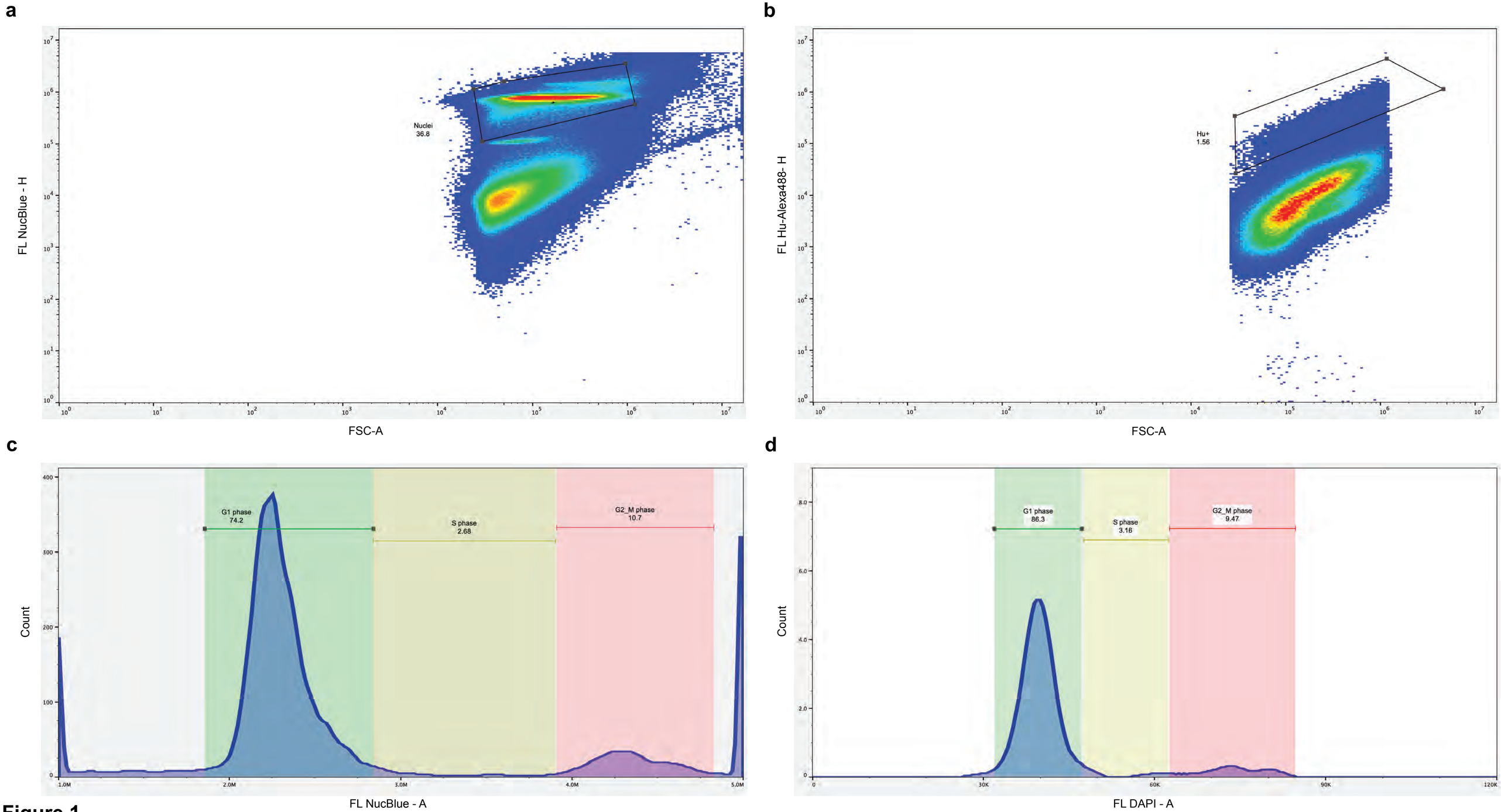
a
Nuclei
36.8
FL NucBlue - H
FSC-A
b
Hu+
1.56
FL Hu-Alexa488- H
FSC-A
c
G1 phase
74.2
S phase
2.68
G2_M phase
10.7
Count
FL NucBlue - A
d
G1 phase
86.3
S phase
3.16
G2_M phase
9.47
Count
FL DAPI - A

Figure 1

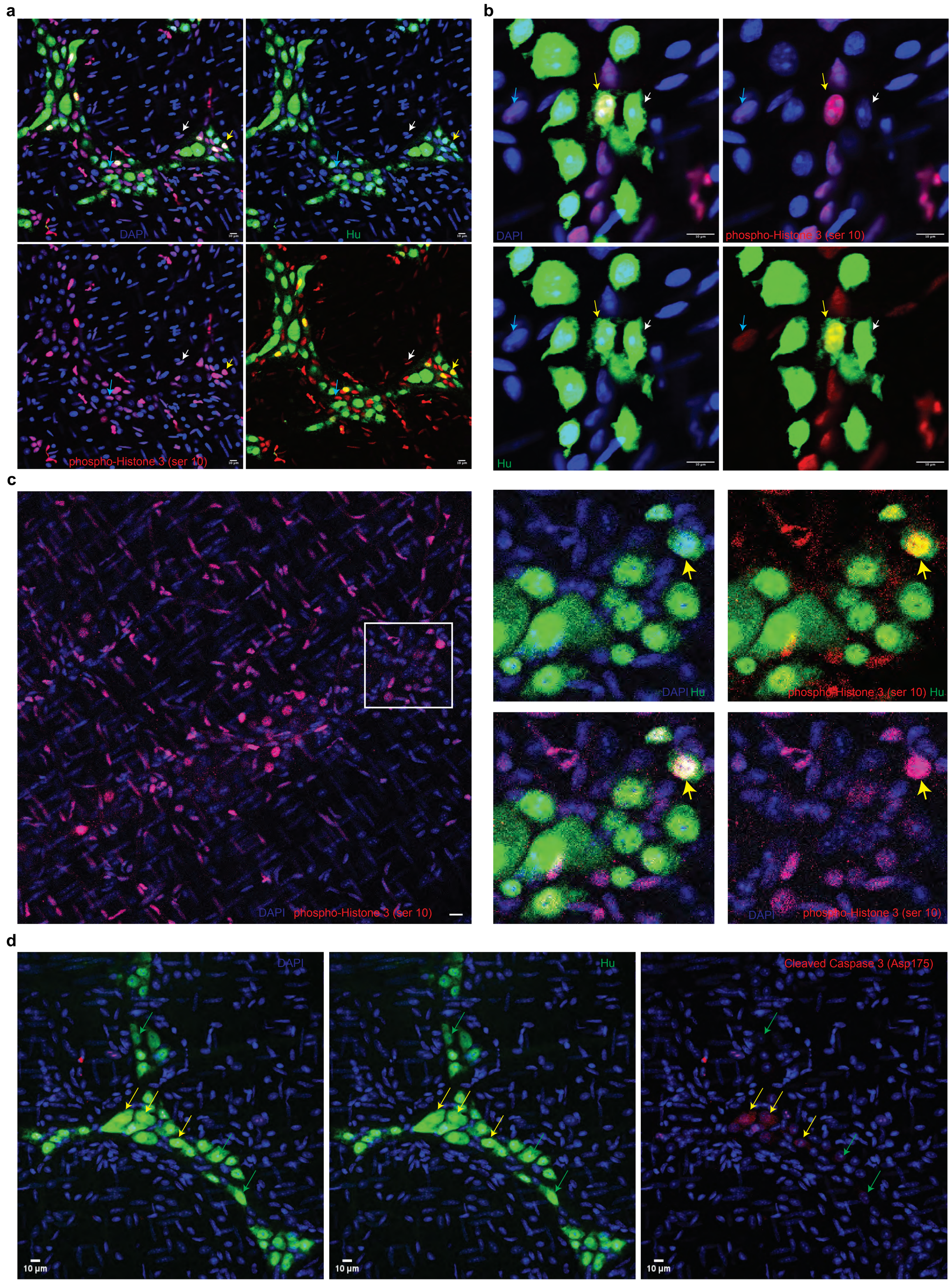
a
DAPI
Hu
phospho-Histone 3 (ser 10)
b
DAPI
phospho-Histone 3 (ser 10)
Hu
c
DAPI phospho-Histone 3 (ser 10)
DAPI Hu
phospho-Histone 3 (ser 10) Hu
DAPI
phospho-Histone 3 (ser 10)
d
DAPI
Hu
Cleaved Caspase 3 (Asp175)
10 µm

Figure 2

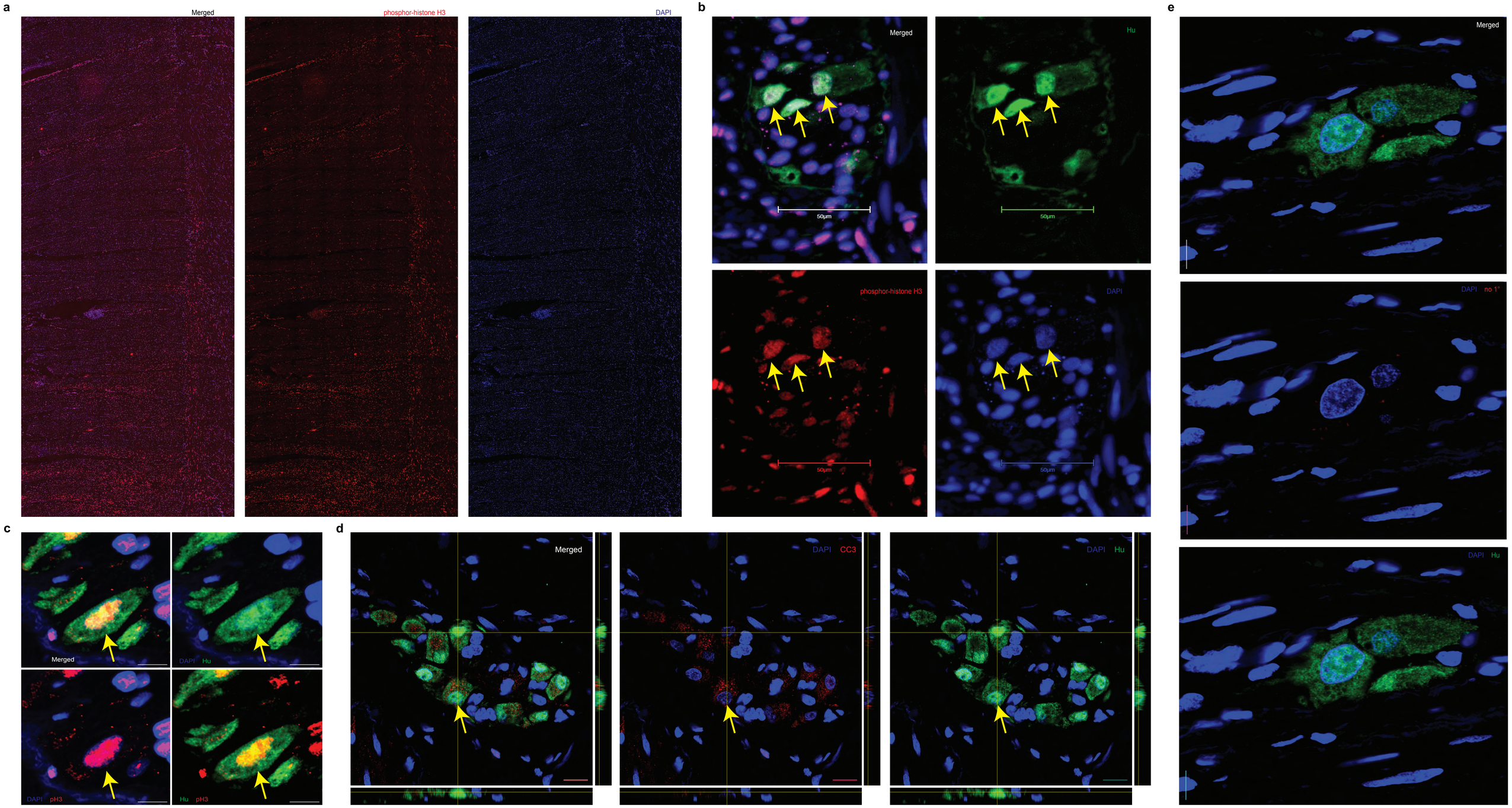
a
Merged
phosphor-histone H3
DAPI
b
Merged
50µm
Hu
50µm
phosphor-histone H3
50µm
DAPI
50µm
e
Merged
DAPI no 1°
DAPI Hu
c
Merged
DAPI Hu
DAPI pH3
Hu pH3
d
Merged
DAPI CC3
DAPI Hu

Figure 3

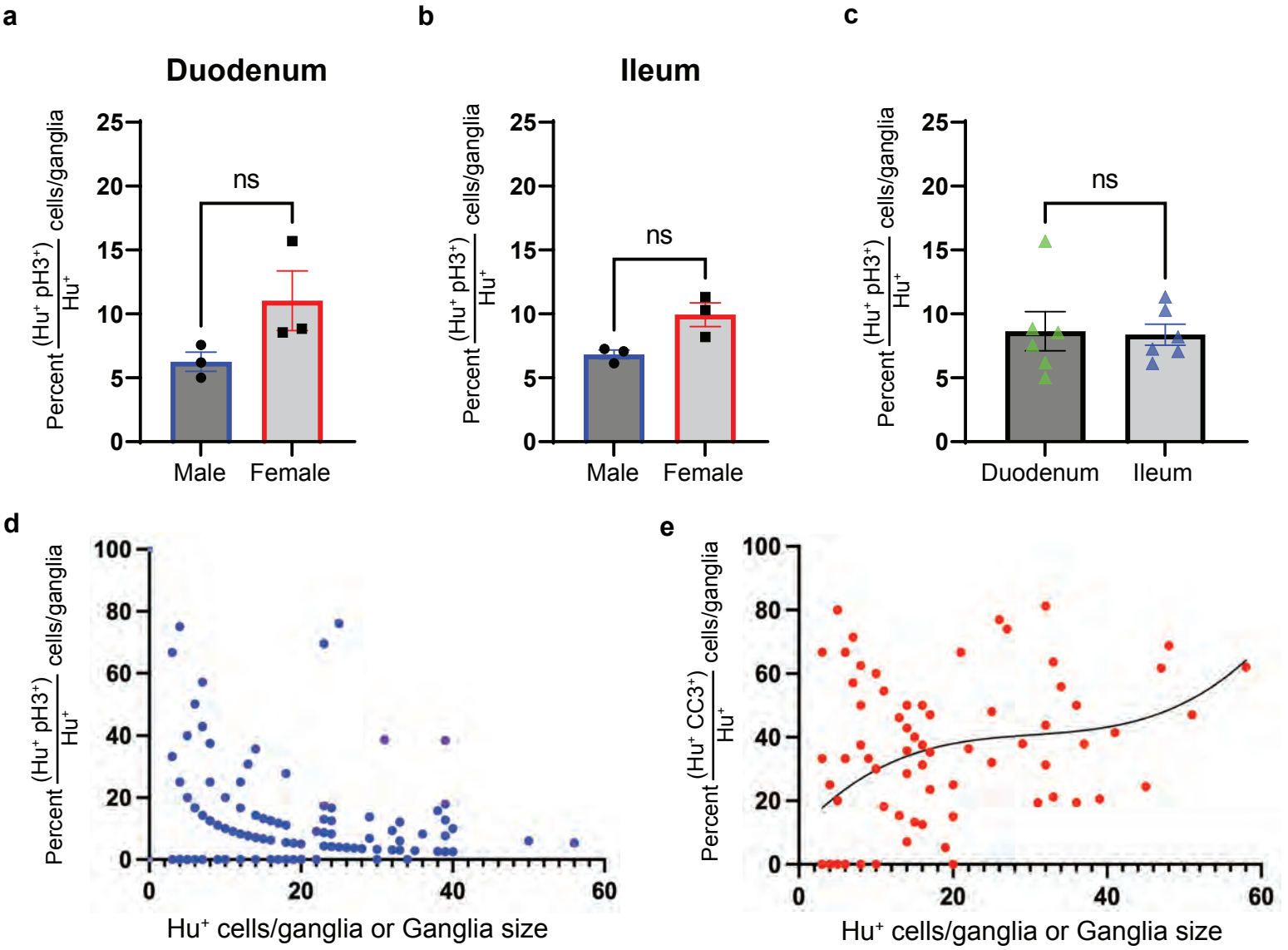
a
Duodenum
Percent (Hu+ pH3+) / Hu+ cells/ganglia
25
20
15
10
5
0
ns
Male
Female
b
Ileum
Percent (Hu+ pH3+) / Hu+ cells/ganglia
25
20
15
10
5
0
ns
Male
Female
c
Percent (Hu+ pH3+) / Hu+ cells/ganglia
25
20
15
10
5
0
ns
Duodenum
Ileum
d
Percent (Hu+ pH3+) / Hu+ cells/ganglia
100
80
60
40
20
0
0
20
40
60
Hu+ cells/ganglia or Ganglia size
e
Percent (Hu+ CC3+) / Hu+ cells/ganglia
100
80
60
40
20
0
0
20
40
60
Hu+ cells/ganglia or Ganglia size

Figure 4

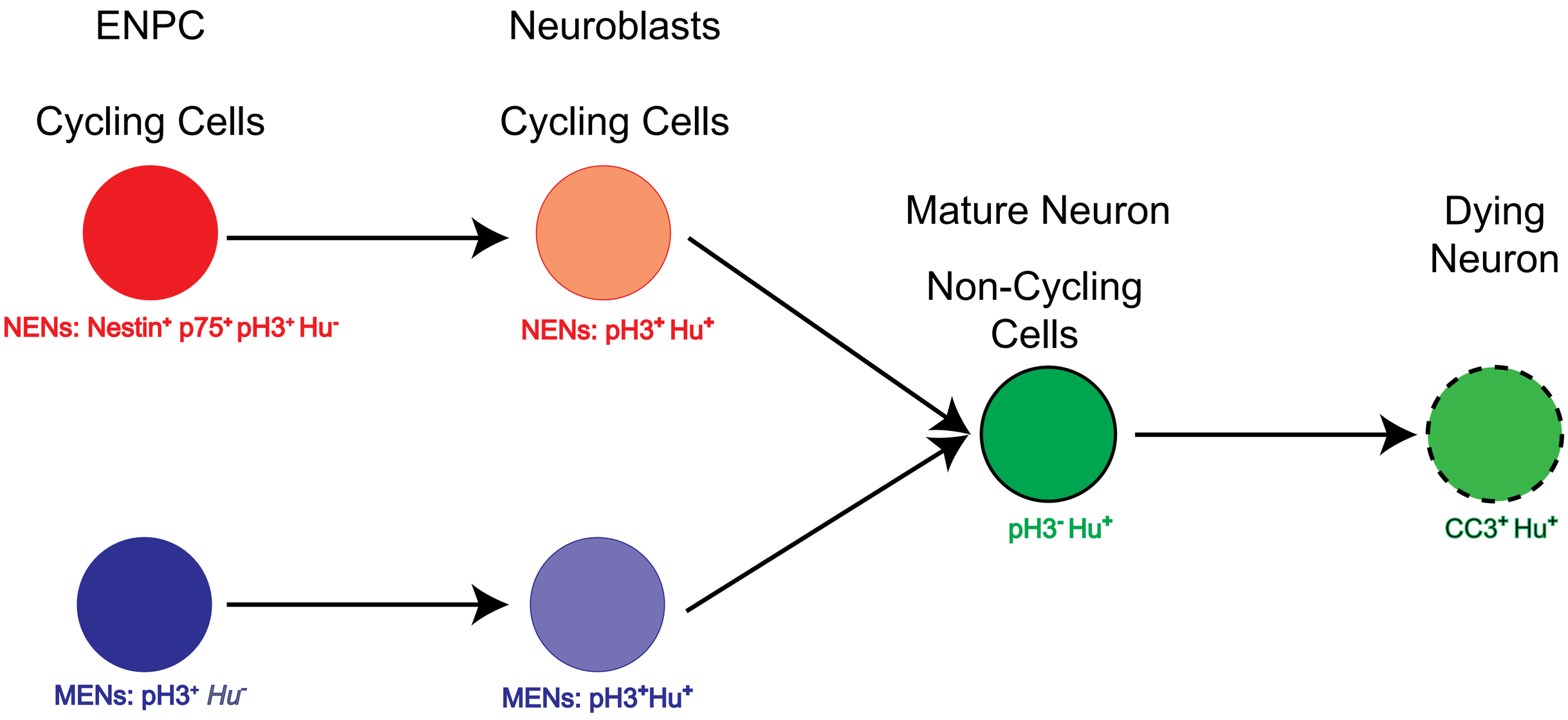
ENPC
Neuroblasts
Cycling Cells
Cycling Cells
Mature Neuron
Dying Neuron
Non-Cycling Cells
NENs: Nestin+ p75+ pH3+ Hu-
NENs: pH3+ Hu+
pH3- Hu+
CC3+ Hu+
MENs: pH3+ Hu-
MENs: pH3+Hu+

Figure 5